Excited State Dynamics of Bistridentate and Trisbidentate Ru^{II} Complexes of Quinoline-Pyrazole Ligands

Inorganic Chemistry
Article
Cite This: Inorg. Chem. 2019, 58, 16354−16363
pubs.acs.org/IC

Excited State Dynamics of Bistridentate and Trisbidentate Ru^{II} Complexes of Quinoline-Pyrazole Ligands

Lisa A. Fredin,[‡,∥,⊥] Joachim Wallenstein,[†,⊥] Elin Sundin,[†] Martin Jarenmark,[§] Deise F. Barbosa de Mattos,[†] Petter Persson,[‡] and Maria Abrahamsson*[,†]

[†]Department of Chemistry and Chemical Engineering, Chalmers University of Technology, SE-41296 Gothenburg, Sweden
[‡]Theoretical Chemistry Division, Department of Chemistry, Chemical Center, Lund University, Box 124, SE-22100 Lund, Sweden
[§]Department of Geology, Lund University, Solvegatan 12, SE-22362, Lund, Sweden

Supporting Information

ABSTRACT: Three homoleptic ruthenium(II) complexes, $[Ru(Q3PzH)_3]^{2+}$, $[Ru(Q1Pz)_3]^{2+}$, and $[Ru(DQPz)_2]^{2+}$, based on the quinoline−pyrazole ligands, Q3PzH (8-(3-pyrazole)-quinoline), Q1Pz (8-(1-pyrazole)-quinoline), and DQPz (bis(quinolinyl)-1,3-pyrazole), have been spectroscopically and theoretically investigated. Spectral component analysis, transient absorption spectroscopy, density functional theory calculations, and ligand exchange reactions with different chlorination agents reveal that the excited state dynamics for Ru(II) complexes with these biheteroaromatic ligands differ significantly from that of traditional polypyridyl complexes. Despite the high energy and low reorganization energy of the excited state, nonradiative decay dominates even at liquid nitrogen temperatures, where triplet metal-to-ligand-charge-transfer emission quantum yields range from 0.7 to 3.8%, and microsecond excited state lifetimes are observed. In contrast to traditional polypyridyl complexes where ligand exchange is facilitated by expansion of the metal−ligand bonds to stabilize a metal-centered state, photoinduced ligand exchange occurs in the bidentate complexes despite no substantial MC state population, while the tridentate complex is extremely photostable despite an activated decay route, highlighting the versatile photochemistry of nonpolypyridine ligands.

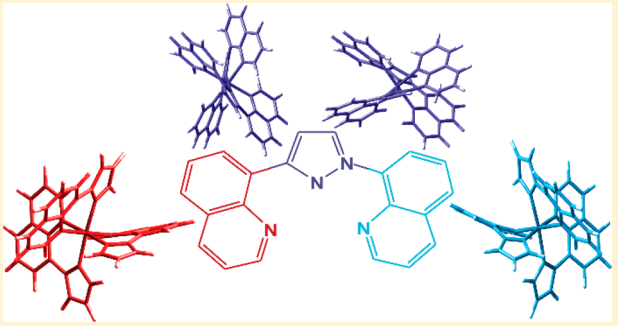

Ru^{II} complexes with polypyridine ligands are frequently used in catalysis,[1−3] as light harvesters,[4,5] and as luminescent probes[6,7] and are proposed for use in drug delivery,[8] as anticancer drugs,[9] and in information storage.[10] Their photophysical properties are governed by an intricate combination of structural and electronic properties.[11−13] Typically, Ru^{II} polypyridyl type complexes exhibit intense visible light absorption, due to the promotion of an electron from a Ru t_{2g} orbital to a ligand π^* orbital, resulting in a singlet metal-to-ligand charge transfer (^{1}MLCT) band. This state undergoes fast intersystem crossing to a ^{3}MLCT state, which is often long-lived (μs) and exhibits excellent photostability.[14−16] Emissive complexes, which often have very small reorganization energy between the excited ^{3}MLCT and the ground state (GS), release excited state energy radiatively as light. In addition to this radiative decay, ^{3}MLCT states can decay nonradiatively via an activated transition to a metal centered (MC) state, as is expected for most polypyridyl complexes,[17] or directly to the GS, especially when the energy of the excited state is low.[18,19] The interplay between the competing decay pathways is well understood for bipyridine complexes but is substantially less investigated for other types of ligands, such as quinolines or combinations of different heterocycles,[11,12,20−22] whose use is consequently hampered by lack of insight.

We have recently shown that combinations of quinoline (Q) and pyrazolyl (Pz) into polyheteroaromatic bidentate ligands (Chart 1) allow formation of homoleptic bidentate complexes

Chart 1. Structures of the QPz Ligands

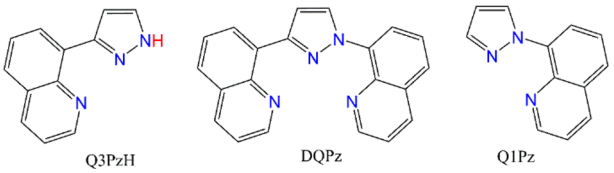

of the type $[Ru(QPz)_3]^{2+}$.[21,23,24] The photoresponse of these complexes is shown to differ depending on whether the Pz and Q motifs are connected in the 1- or 3- position of Pz.[24] The *mer*- and *fac*- isomers of the homoleptic complexes of Q3PzH and Q1Pz can be separated, as the *fac*- isomer is more susceptible to photoinduced ligand loss.[21,23] Both *mer*-complexes also undergo visible light photoinduced ligand-solvent-exchange in acetonitrile.[21] Adding triflic acid leads to a decrease in the MLCT bands (300−600 nm) and a growth of a

Received: June 5, 2019
Published: December 4, 2019

DOI: 10.1021/acs.inorgchem.9b01543
Inorg. Chem. 2019, 58, 16354−16363

new band at 380 nm producing two distinct isosbestic points for each complex. These changes in absorption and new resonances in the ^{1}H NMR spectra indicate dechelation of only the quinoline as the rate-limiting step.[21] A tridentate ligand analogue with two Q and one Pz (DQPz, Chart 1) also forms a Ru^{II} complex, which undergoes room temperature dynamic interconversion between two ground state diastereomers.[24] The interconversion was attributed to a mechanism involving a large scale twisting motion of the ligands, with a transition barrier of ~70 kJmol^{-1} for the diastereomerization.[24]

Ru complexes are used in complex salt environments, so understanding how the structure and properties of a complex change upon irradiation, temporarily or permanently, is crucial to designing complexes for photocatalytic or dye-sensitization applications that often occur in a complex matrix. In particular, the mechanistic insight into Ru−Cl coordination is critical to the performance of Ru-based water oxidation catalysts.[25−27] Particularly, $[Ru(bpy)_2(L)]^{2+}$ where L is en (ethylenediamine) or dae (1,2-dianilinoethane) was shown to have ~0.2% photoconversion to $Ru(bpy)_2Cl_2$ in the presence of Cl^-.[28] A recent systematic study of phosphonic acid Ru^{II} polypyridyl sensitizers shows that ligand bulkiness, hydrophobicity, and electron-donating groups affect the desorption and decomposition of the dye via photodissociation of a ligand.[29] Similarly, it has been shown that more efficient photodissociation of pyridine can be achieved by increasing the bulkiness of one ligand, L, in complexes of the type $[Ru(tpy)(py)(L)]^{2+}$ where tpy is 2,2′:6′,2″-terpyridine; py is pyridine; and L is bpy (bipyridine), dmb (4,4′-dimethyl-2,2′-bipyridine), or biq (2,2′-biquinoline).[30] While these studies provide design rules for pyridine ligands, their applicability to polyheteroaromatic or nonpyridine ligands is currently unknown.

Here, we report a detailed comparative study including experimental photophysical data and density functional theory (DFT) calculations for a series of inter-related biheteroaromatic meridional (*mer*) isomers (Chart 2), $[Ru(Q3PzH)_3]^{2+}$ (**1**), $[Ru(Q1Pz)_3]^{2+}$ (**3**), and $[Ru(DQPz)_2]^{2+}$ (**2**), and contrast them to other complexes with Q-type ligands. Characterization of the nature and deactivation of their excited states and the excited state reactivity of each complex with Cl^- provides a systematic assessment of excited state properties of complexes based on quinoline−pyrazole combination ligands.

Chart 2. Structures of the *mer*-$[Ru(Q3PzH)_3]^{2+}$, *mer*-$Ru(DQPz)_2]^{2+}$, and *mer*-$[Ru(Q1Pz)_3]^{2+}$

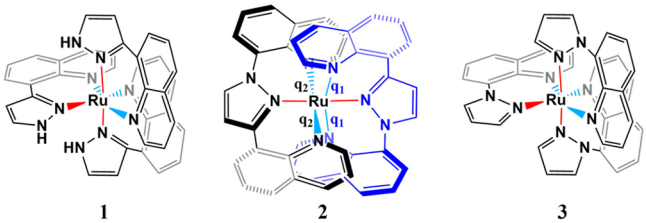

1 2 3

METHODS

Experimental Section. The complexes were available from a previous study,[21] and the syntheses are reported in **1**,[23] **3**,[21] and **2**,[24] along with the crystal structures of **1**[23] and **2**.[21] No suitable crystals were ever grown of **3**. Solvents were all spectrophotometric grade and purchased from Sigma-Aldrich; water was deionized and filtered through a Milli-Q system (Advantage A10). Sodium chloride (>99.5%) and tetrabutylammonium chloride (>97%) were purchased from Sigma-Aldrich, and hydrochloric acid (34%) was bought from Merck.

Spectroscopy. Temperature-dependent emission samples were prepared with an optical density (OD) of 0.1 at the excitation wavelength (room temperature). All temperature dependent measurements were performed in a liquid nitrogen cooled cryostat (Optistat, Oxford Instruments), and the temperature was monitored and controlled by a thermal control unit (ITC4, Oxford Instruments). Ramp rates were 1 K/min maximum below 180 K. Each measurement was taken after ~30 min equilibration at the given temperature. Temperature dependent absorption spectra were recorded with a Varian Cary 5000 UV/vis−NIR (Varian, US).

Steady-state emission spectra were recorded on a Jobin-Yvon SPEX 3, with either an R928 or an R2608 photomultiplier tube, and the spectra were corrected by the software to account for the wavelength dependence of the detectors. Spectrophotometric grade solvents were used, and deoxygenation was achieved with ~10 min of Ar purging before sealing the 10 × 10 mm high neck fluorescence cuvettes. Quantum yields of emission, with $[Ru(bpy)_3]Cl_2$ as a reference, were calculated in the wavenumber regime according to

$$\Phi = \Phi_{ref} \times \frac{A_{ref}}{A} \times \frac{\int I(\nu)\, d\nu}{\int I_{ref}(\nu)\, d\nu} \times \frac{\eta^2}{\eta_{ref}^2} \quad (1)$$

where Φ is the quantum yields of emission, A is the absorbance at the excitation wavelength, $I(\nu)$ is the intensities, and η is the refractive indices of the sample and reference. The refractive index for the 1:4 methanol−ethanol mixture was 1.452, taken as a geometrical mean at 77 K (1.418 and 1.461, respectively).[31] Rate constants were calculated as $k_{rad} = \Phi/\tau$ and $k_{nr} = (1 - \Phi)/\tau$.

Spectral component analysis was carried out using a home written Matlab program, following the approach of Meyer.[17,32−35] The emission spectra can be fitted to a series of Gaussians according to

$$E(\nu) = \sum_{n_m} \sum_{n_l} ((E_{00} - \nu_m n_m - \nu_l n_l)/E_{00})^4 \left(\frac{S_m^{n_m}}{n_m!}\right)\left(\frac{S_l^{n_l}}{n_l!}\right) \times e^{(-4\ln(2)((\nu - E_{00} + \nu_m n_m + \nu_l n_l)/\Delta\nu_{1/2})^2} \quad (2)$$

Table 1. Photophysical Parameters: Low Temperature Maximum Intensity Emission Wavelength (λ_{Em}), Excited State Lifetime (τ), Quantum Yield (Φ), Radiative (k_{rad}) and Nonradiative Rate Constants (k_{nr}), and Room Temperature Time Constants Extracted from TA Measurements

	77 K (MeOH/EtOH)					298 K (MeCN)	
compound	λ_{em} (nm)	$\tau(\mu s)$	Φ (%)	$k_{rad}(\times 10^3\ s^{-1})$	$k_{nr}(\times 10^5\ s^{-1})$	τ_1(ns)	τ_2 (ns)
1	696	4.99	0.7	1.4	2.0	0.23 ± 0.01 (<5%)	<0.0002
3	676	7.06	1.4	1.9	1.4	7.3 ± 2.3 (27%)	0.12 ± 0.08 (73%)
2	680	5.73	3.8	6.6	1.7	5.8 ± 0.98 (40%)	0.77 ± 0.05 (60%)
$[Ru(bpy)_3]^{2+}$,[15]	582	5.1	33	60	1	1150	
$[Ru(tpy)_2]^{2+}$,[53]	598	11	48	40	0.5	0.25[54]	
$[Ru(DQP)_2]^{2+}$,[42]	673	8.5	0.06	7[43]	1[43]	3000	

DOI: 10.1021/acs.inorgchem.9b01543
Inorg. Chem. 2019, 58, 16354−16363

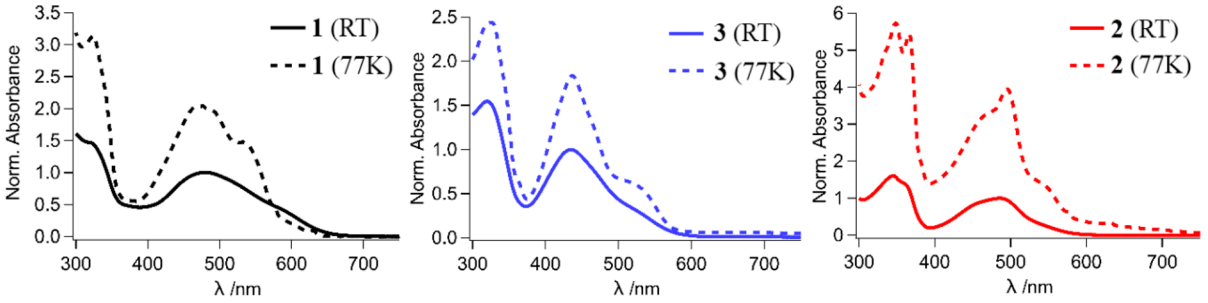

Figure 1. Temperature dependent MLCT absorption of complexes in MeOH/EtOH (1:4, v/v), at ambient temperature (solid) and in a solid matrix at liquid nitrogen temperature (dashed). Normalized with respect to λ_{max} at ambient temperature. More temperature steps are shown in Figures S1–S3.

where ν is the emission energy (cm^{-1}), $E(\nu)$ is the recorded emission intensity at ν, E_{00} is the energy of the 0–0 transition, and $\Delta\nu_{1/2}$ is the full-width-half-maximum (fwhm) of the Gaussians. ν_m and ν_l are the medium and low frequency vibrational transitions, and n_m and n_l are their corresponding quantum numbers. S_m and S_l are the Huang–Rhys factors and provide a quantitative measure of the distortion between the ground and excited state and are related to the reorganization energy.[35,36] Initial guesses were made for S_m, E_{00}, and ν_m based on spectral shape.[32] The parameters were constrained to vary: $\nu_{1/2}$ [500–1500 cm^{-1}], S_l and S_m [0.1–4], ν_m [1000–1500 cm^{-1}], and ν_l [250–750 cm^{-1}]. The parameters obtained from the fitting are given in Table 1, and the spectra with the resulting Gaussians are in Figures S9–S11.

In nanosecond transient absorption spectroscopy, the doubled fundamental, 532 nm, from a Nd:YAG laser (Sure-Lite), was attenuated and directed to the sample (7 ns fwhm, 10 Hz, 16 mJ/pulse). As the measurements were taken in a solid matrix, the susceptibility toward ligand exchange is expected to be less pronounced. With a spot size of ~1 cm wide at a 10 Hz repetition rate, there was no change observed in the absorption before and after the measurements at 80 K (as seen for **1** in Figure S12). Probe light is supplied by a 250 W tungsten lamp housing (Newport, model 67009), and probe and detector monochromators (Newport, model 74004) were used for wavelength selection. The transmitted light was recorded by a five-stage PMT (Applied Photophysics, model C00699) and the signal processed via oscilloscope (Tektronix TDS2122) and digitized using a homemade analogue-to-digital-converter. All complexes displayed self-consistent monoexponential decays (as indicated by the kinetic traces shown in Figure S14) at all wavelengths, and the excited states were formed within the pulse width (~10 ns fwhm).

In the photolysis experiments, absorption spectra of the complexes in micromolar solutions were recorded on a Varian Bio Cary 50, while a Xe-arc lamp was used for irradiation. The light from the Xe-arc lamp was filtered through a long-pass filter (blocking λ < 455 nm), as well as an IR filter (blocking λ > 800 nm), to avoid heating. Spectra were collected every 12 s.

A home-built pump–probe setup was used to record fs transient absorption spectra and decays. The samples were measured in air equilibrated MeCN in 2 mm cuvettes, and the absorbance was adjusted to ~0.5 at the excitation wavelength. A Ti:sapphire oscillator (Tsunami, Spectra Physics), generating pulses around 100 fs broad (fwhm), was used to seed a Ti:sapphire regenerative amplifier (Spitfire, Spectra Physics) that was pumped by a frequency-doubled diode-pumped Nd:YLF laser (Evolution-X, Spectra Physics) and produced pulses of approximately 200 fs duration (fwhm) at a 1 kHz repetition rate. After the regenerative amplifier, the amplified laser beam (800 nm) was split by a beamsplitter, and the two beams were used as pump and probe light. The pump beam wavelength was tuned by an OPA (TOPAS, Light Conversion Ltd.) to yield 490 nm and was delayed relative to the probe light using an optical delay stage (range 0–10 ns). White light was generated in a CaF_2 plate (400–780 nm). The white light was then divided into one reference and one probe beam respectively, and the probe light was overlapped with the pump light (2 mW, spotsize ~0.4 mm) at the sample. The probe and reference light were focused on the entrance slit of a spectrograph and detected by a CCD camera (iXon-Andor) operating synchronously with the 1 kHz laser. The transient spectra were obtained from the difference of the probe light divided by the reference with and without excitation of the sample by the pump beam; 2000 spectra were averaged per delay time using a homewritten LabVIEW program. The excited state lifetimes were extracted from fits to a sum-of exponentials using the function $I(t) = \sum_i A_i \exp(-t/\tau_i)$. Three different wavelengths were fitted for each complex, from which an average lifetime and standard deviation was obtained. The amplitudes were also reported as average values from the three wavelengths. The fitting was executed using a Matlab program, where minimizing was achieved using the least-square method. A biexponential function was sufficient for complexes **1** and **3**, while **2** required a third component to account for the rise of the signal.

Density Functional Theory. The relaxed ground state electronic structure of **1**, **3**, and the C–R_a and C–S_a isomers of **2** were optimized using the widely used PBE0[37–39] functional in conjunction with standard Gaussian type orbital (GTO) basis sets of double-ζ quality, 6-31G(d,p), and the SDD Stuttgart/Dresden effective core potential (ECP) was used to provide an effective core potential for Ru[40] with a complete polarizable continuum model (PCM) solvent description for acetonitrile. All calculations were performed using the Gaussian 09 program[41] with a total charge on the complex (+2). The fully optimized minima were run with no symmetry constraints applied and standard convergence criteria, allowing for possible Jahn–Teller effects. The potential energy curves (Figure S27) are formed by constraining the Ru–ligand bonds at various lengths between the 2.05 Å and ~2.75 Å and optimizing the rest of the structure.

RESULTS AND DISCUSSION

The Excited State Manifold. The UV–vis spectra of **1** and **3** have been previously reported.[21,23] However, the variation in their absorption spectra in MeCN and H_2O, and their oxidation and reduction potentials, indicates that the excited state properties differ, despite similar GS orbital structures. Therefore, here, the temperature dependent absorption and emission along with spectral component analysis, transient absorption spectroscopy, and density functional theory calculations are used to characterize the excited state landscape of each complex.

Temperature dependent UV–vis absorption of the *mer*-isomers in MeOH/EtOH (1:4 v/v) show room temperature MLCT spectra (Figure 1) that are similar to those reported in acetonitrile (Figure S4).[21,23] However, **1** exhibits a broad shoulder at ~575 nm (which can be seen more clearly in Figure S1), which was attributed to a partly deprotonated complex as a similar shoulder grows after adding a base in MeCN.[21,23] Upon cooling, the shoulders observed at room temperature become more pronounced, Figure 1.

DOI: 10.1021/acs.inorgchem.9b01543
Inorg. Chem. 2019, 58, 16354–16363

In contrast to the seminal complex $[Ru(bpy)_3]^{2+}$ which is known for its long-lived ^{3}MLCT state, none of the complexes investigated here display any emission at room temperature, either in steady state or single photon counting measurements. Room temperature femtosecond transient absorption (TA) data reveal short-lived excited states for all complexes. For **2**, data are shown in Figure 2. The fs-TA spectra were similar for

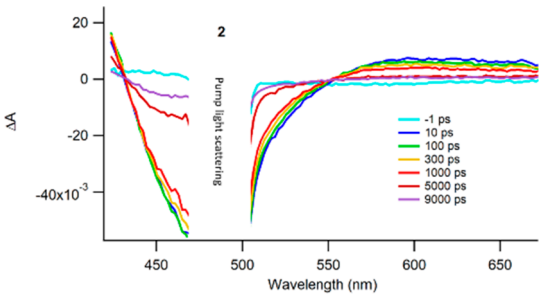

Figure 2. fs-transient absorption spectra excited at 490 nm for **2** recorded in MeCN. The region around 490 nm is not shown due to scattering from the pump light. Femtosecond transient absorption spectra of **1** and **3** can be found in Figures S16 and S17. Figure S18 shows representative biexponential fits for **1**–**3**.

all complexes, exhibiting the expected ground state bleach in the MLCT absorption region and a broad, weak excited state absorption feature above 550 nm, also typical for Ru(II)-polypyridine type complexes.[44,45] The ground state bleach is largely obscured by the scattering from the excitation pulse, which precludes any detailed comparisons between the complexes; suffice it to say that the isosbestic point is slightly blue-shifted for **3** compared to **1** and **2** (see Figure S19). The same spectral features are observed at liquid nitrogen temperatures (Figures 2, S13, S16, S17, and S19), confirming the MLCT nature of the lowest excited state. All complexes display uniform decay over the whole spectral range investigated, and a sum of exponentials was needed to adequately describe the decay (see Experimental Section). In the ns-TA at 77 K, strong positive features at higher energies with intensities comparable to the MLCT bleach (Figure S13) can be attributed to the reduced ligands.[16,46] Excited state lifetimes were obtained from the fits to the decay of the MLCT excited state absorption band (Figure S18), and the average lifetime decreases in the order 2 > 3 > 1, correlating well with the extracted radiative and nonradiative rate constants (Table 1), *vide infra*. Both **2** and **3** display double exponential decay at room temperature with both a nanosecond (≈ 6–7 ns) and a picosecond component, whereas **1** exhibits biexponential decay with the main component in the ultrafast time regime. The origin of the two different lifetimes is unclear, but for **2** they may arise from the different conformers but could also possibly arise from processes such as solvent relaxation, intramolecular vibrational energy redistribution, and intersystem crossing as noted by Damrauer et al.[45] and have previously been observed for $Ru(bpy)_3$.[44] In any case, the fs-TA spectral shapes, corroborated by low-temperature ns-TA, indicate that the longest lifetime for each complex is indeed originating from a short-lived ^{3}MLCT state.

A common reason for not observing a long-lived, emissive ^{3}MLCT state is efficient nonradiative deactivation through a thermally accessible ^{3}MC state.[47−49] These triplet excited states have been characterized using DFT calculations. **1**[23] and **3** both show increased twisting around the Ru center (Table 2) in the ^{3}MLCT state with an electron localized on a single

Table 2. Calculated Energy and Geometry Factors of 1, 3, and the C−Ra and C−Sa Isomers of 2[a]

complex		quantity	GS	^{3}MLCT	^{3}MC
1[19]		E (eV)	0.00	1.96	1.89
		q_{Pz}[b]	2.05 ± 0.01	2.05 ± 0.01	2.09 ± 0.05
		q_Q[b]	2.13 ± 0.02	2.10 ± 0.08	2.39 ± 0.24
		R_{tot}[b]	2.09 ± 0.05	2.08 ± 0.06	2.24 ± 0.23
		O[c]	3.41	3.57	8.03
3		E (eV)	0.00	1.97	1.81
		q_{Pz}[b]	2.06 ± 0.02	2.07 ± 0.01	2.09 ± 0.04
		q_Q[b]	2.12 ± 0.03	2.11 ± 0.09	2.57 ± 0.56
		R_{tot}[b]	2.09 ± 0.04	2.09 ± 0.06	2.33 ± 0.44
		O[c]	2.64	3.16	9.56
2	C−R_a	E (eV)	0.00	1.90	1.88
		q_1[d]	2.10	2.10	2.26
		q_2[d]	2.10	2.08	2.12
		q_{Pz}[b]	2.10	2.10	2.26
		q_Q[b]	2.10	2.08	2.12
		R_{tot}[b]	2.07 ± 0.05	2.06 ± 0.06	2.14 ± 0.13
		O[c]	1.33	2.52	5.34
		P[c]	27.86	28.25	33.32
	C−S_a	E (eV)	0.00	2.26	1.86
		q_1[d]	2.10	2.09	2.41
		q_2[d]	2.10	2.09	2.12
		q_{Pz}[b]	2.00	2.01	2.05
		q_Q[b]	2.10	2.09	2.26
		R_{tot}[b]	2.07 ± 0.02	2.06 ± 0.01	2.19 ± 0.06
		O[c]	1.18	1.11	5.77
		P[c]	27.50	26.77	33.14

[a]Distances in Å and angles in degrees. Deviations calculated as σ_n values. [b]Average bond distances of all Ru−N bonds, Ru−(N)Pyrazole (red in Chart 2) and Ru−(N)Quinoline (light blue in Chart 2; R_{tot}, q_{Pz}, and q_Q). [c]Octahedricity (O) and planarity (P) factors calculated as the root-mean-square error from ideal ligand bond angles, where ideal ligand−Ru−ligand bond angles in an octahedron are 90° and would result in an O of 0 and the ideal ligand dihedral angles are 0° (or flat ligands) and would lead to a P of 0. [d]Average Ru−(N)Quinoline bonds on each ligand, i.e., the blue Ru−Q bonds averaged and black Ru−Q bonds as labeled in Chart 2.

ligand (Figure S24). In the ^{3}MC state, both **1** and **3** have populated a Ru $d_{x^2-y^2}$ orbital with major twisting in the ligand backbones. In **1**, all of the ligands have significant dihedral angles of 36–60°, whereas in **3** the ligands along the Q−Q axis have large ∼35° dihedral angles while the third ligand is much flatter (dihedral ∼15°) resulting in more twisting around the Ru-core itself (less octahedral bonding angles around the metal center, larger O[50,51] in Table 2, Figure S25).

2 has two isomers, C−R_a and C−S_a, that are dynamically present in the ground state at room temperature,[24] and both were characterized. The two ^{3}MLCT states are very similar to electron density on both ligands, where the greater spin overlap between the two ligands in C−S_a (spin densities in Figure S24 and S26) results in a lower energy excited state. The freely optimized ^{3}MC of C−R_a and C−S_a, where a d_{z^2} orbital on each has been populated aligned with the Pz−Pz axis or a Q−Q axis on one ligand, respectively, makes them look quite different along the q_1 (Ru−Q bond lengths on ligand 1) axis shown in Figure 3. However, constrained potential energy scans along q_1 for each isomer (Figure S27) look very similar.

DOI: 10.1021/acs.inorgchem.9b01543
Inorg. Chem. 2019, 58, 16354−16363

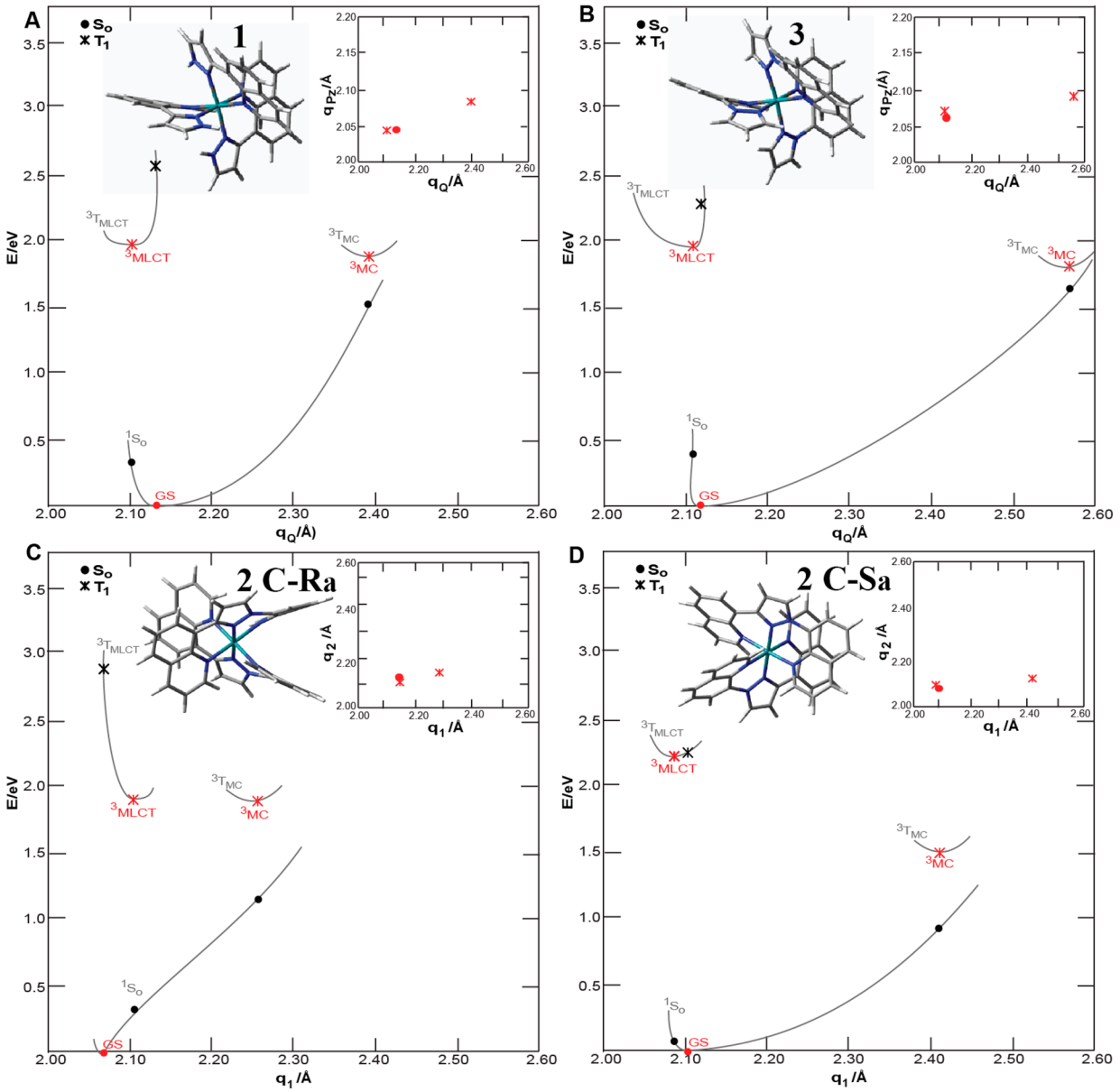

Figure 3. Projected potential energy surfaces (PPES) for (a) **1**,[19] (b) **3**, and the (c) C−Ra and (d) C−Sa isomers of **2**. Singlets and triplets are circles and stars, respectively. The red points are fully optimized minima and the black are the energies on the other surface at these geometries, and the gray surfaces are qualitatively drawn to connect points of similar spin based on the Ru Mulliken spin density. The insets show the optimized ground state structure of each complex and the geometries along both Ru−ligand bond averages relevant for each complex (defined in Table 2).

As triplet surfaces tend to be flatter than the ground state surface, it is not surprising that the triplet transition state shows a lower activation barrier of 0.1 eV for C−R_a to C−S_a conversion (Figure S26), whereas the C−S_a to C−R_a ground state activation barrier is ∼0.8 eV. These relatively low interconversion barriers and the breadth of ^{3}MC geometries found (both with Ru−Q expansions and Ru−Pz expansions) are indicative of many possible ^{3}MLCT to ^{3}MC pathways for **2**.

The lack of room temperature emission and the short-lived MLCT states observed in fs-TA suggest that the MC state may be easily accessible from the ^{3}MLCT potential energy surface for each complex. If the MC is accessible, the relatively low calculated ^{3}MC energies, compared to $[Ru(DQP)_2]^{2+}$'s (DQP is 2,6-di(quinolin-8-yl)pyridine) relaxed ^{3}MC energy ∼2 eV,[52] point to fast nonradiative decay from the ^{3}MC state for all three, as is typically expected for bistridentate Ru^{II} complexes.[15,53] In addition, the calculated ^{3}MLCT energies indicate a relatively low ^{3}MLCT-GS energy gap and therefore significant nonradiative decay directly to the ground state[18,19,54] (for reference, $[Ru(DQP)_2]^{2+}$'s relaxed ^{3}MLCT energy is ∼2.2 eV[52]). This would be consistent with the lack of room temperature emission.

Radiative and Nonradiative Decay Processes. Despite the lack of room temperature emission, low temperature emission data can provide valuable insight into both radiative and nonradiative decay pathways. At liquid nitrogen temperatures in MeOH/EtOH glass, all complexes show broad emission between 630 and 900 nm, which is consistent with ^{3}MLCT emission (Figure 4).[14,15] The bidentate complexes displayed broad and unstructured emission with maximum intensity at 695 and 675 nm, respectively, while **2** exhibited

DOI: 10.1021/acs.inorgchem.9b01543
Inorg. Chem. 2019, 58, 16354−16363

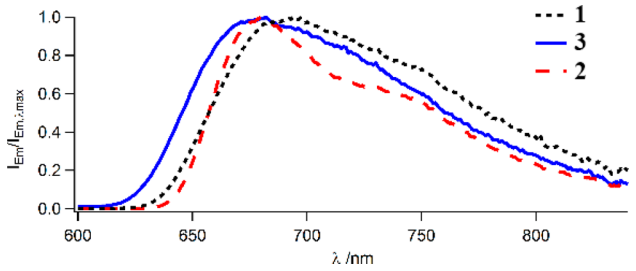

Figure 4. Corrected emission spectra of **1**, **3**, and **2** in MeOH/EtOH glass at 77 K probed at the MLCT maxima with 475, 450, and 495 nm light, respectively. Detailed temperature studies in Figures S6–S8.

additional vibrational structure[12,13,59–62,15,17,32,33,55–58] (more obvious in the wavenumber regime shown in Figure S5) with maximum emission intensity at 675 nm and a second pronounced peak at lower energy (Figure S8 and vibrational components Figure S11). The photoluminescence quantum yields at 77 K were estimated using comparative actinometry as explained in the Methods section. **2** was the strongest emitter with Φ = 3.8%, while **1** and **3** displayed a Φ of 0.7% and 1.4%, respectively. These yields are an order of magnitude lower than what is typically observed for Ru–polypyridine complexes at 77 K.[15]

To detangle the variations in the radiative and nonradiative deactivation of the excited state, we used spectral component analysis of the time-resolved emission at 77 K using the approach introduced by Meyer[17,32–35] (detailed in the Methods section) and compared the results with available literature data. The shape of the emission spectra can be correlated to the ^{3}MLCT-GS energy gap (E_{00}), the vibrational spacing of the accepting modes (medium and low frequency, ν_m and ν_l), and the distortion along these modes (Huang–Rhys factors, S_m and S_l) by fitting a set of Gaussians whose full-width-half-maximum ($\Delta\nu_{1/2}$) best describe the observed spectra (Table 3).[35,36]

The obtained ν_m values are very similar and within what is to be expected from both prototypical polypyridyls like $[Ru(bpy)_3]^{2+}$ and $[Ru(tpy)_2]^{2+}$,[17] and what has been reported for $[Ru(DQP)_2]^{2+}$.[43] However, the energy gap and $\Delta\nu_{1/2}$ are distinctly different from those of $[Ru(bpy)_3]^{2+}$ and $[Ru(tpy)_2]^{2+}$.[17] E_{00} falls in the range ~14 800–15 200 cm^{-1}, which is in good agreement with calculated Δ^3MLCT-GS energies of ~1.9 eV for all three complexes (using the lowest energy isomer of **2**). These transitions are ~1000 cm^{-1} lower in energy than $[Ru(bpy)_3]^{2+}$ and $[Ru(tpy)_2]^{2+}$ but similar to what has been reported for $[Ru(DQP)_2]^{2+}$, corresponding to an emission energy red-shift for Q-containing complexes (Table 1).[43] The half widths, $\Delta\nu_{1/2}$, of the two bidentate complexes differ by ~130 cm^{-1} (Table 3) and are roughly double those of the polypyridyls. A comparison with the $[Ru(bpy)_2(QPy)]^{2+}$-type[12] and $[Ru(DQP)_2]^{2+}$-type[43] complexes suggests that the inclusion of the quinoline group may be the reason for the large half widths. Interestingly quinolines seem to lead to a flatter ^{3}MLCT surface,[63,64] possibly indicating the larger half width might be due to a larger distribution of degenerate ^{3}MLCT structures obtained after the vertical excitation and quick intersystem crossing to the triplet surface. Notably, both ν_l and the Huang–Rhys factors differ markedly between the bi- and tridentate complexes. This is in good agreement with the smaller calculated distortion between the GS and ^{3}MLCT in **2** than in **1** and **3**, which can be understood both in terms of the ability to delocalize the electron density over a larger ligand and the higher rigidity provided by the tridentate chelate.[27] In addition, this smaller ^{3}MLCT-GS reorganization for **2** aligns with its higher emission yield. Interestingly, the much lower emission yield of **1** might be due to the NH overtone on the ligands promoting intersystem crossing from the ^{3}MLCT state to the GS ground state as seen in other complexes with NH groups.[65,66]

Due to its similarity to the bis-tridentate $[Ru(DQP)_2]^{2+}$, one might have expected **2** to exhibit strong photoluminescence at room temperature.[11,42] A brief comparison between $[Ru(DQP)_2]^{2+}$ and **2** reveals a 20 nm blue-shift in emission energy for **2** and radiative rate constants that are almost equal (~7 × 10^3 s^{-1}),[43] which are an order of magnitude lower than what is typically observed for Ru–polypyridine complexes[15] indicating that Q groups suppress radiative decay. Interestingly, both **1** and **3** started emitting around 180 K, while **2** required lower temperatures before the same emission intensities could be readily detected (Figures S6–S8). This observation is in good agreement with the relatively low-lying ^{3}MC states of each complex but the significantly lower ^{3}MLCT-GS and ^{3}MLCT-^{3}MC reorganization of **2** revealed in the calculations. In addition, the quantum yields and calculations imply that at elevated temperatures the nonradiative decay of the excited state of **2** is substantially higher than for the trisbidentate complexes. This is supported by the calculated projected potential energy surfaces (Figure 3), which show relatively small displacement (in q_1) between the ^{3}MLCT and ^{3}MC states in **2** C–R$_a$, implying the existence of fast MC-mediated deactivation pathways.

Overall, the nonradiative rate constants are roughly 2–3 times higher in the biheteroaromatic complexes reported here than for prototypical polypyridyl complexes. Furthermore, they are 2 orders of magnitude larger than the radiative rate constants, making the nonradiative deactivation the majority decay pathway for all the complexes (Figure 5).

Excited State Reactivity. The tridentate complex, **2**, appears to be almost as photostable as the $[Ru(DQP)_2]^{2+}$

Table 3. Spectral Component Analysis Parameters of Spectra Recorded in 77 K MeOH/EtOH (1:4 v/v) Glass[a]

	E_{00} (cm^{-1})	$\Delta\nu_{1/2}$ (cm^{-1})	ν_m (cm^{-1})	ν_l (cm^{-1})	S_m (cm^{-1})	S_l (cm^{-1})
1	15 050	1346	1319	457	0.81	1.92
3	15 269	1479	1263	452	0.85	1.68
2	14 827	1326	1368	604	0.68	0.88
$[Ru(bpy)_3]^{2+}$[12]	17 200	650	1350	400	0.87	0.97
$[Ru(tpy)_2]^{2+}$[12]	16 000	540	1300	400	0.53	0.92
$[Ru(DQP)_2]^{2+}$[45]	14 950	1330	1330	670	0.99	0.89

[a]Energy (E_{00}) and fwhm ($\Delta\nu_{1/2}$) of the 0–0-transition, medium, and low frequency energies (ν_m/ν_l) and Huang Rhy's factors (S_m/S_l), compared with a set of reference complexes.

DOI: 10.1021/acs.inorgchem.9b01543
Inorg. Chem. 2019, 58, 16354–16363

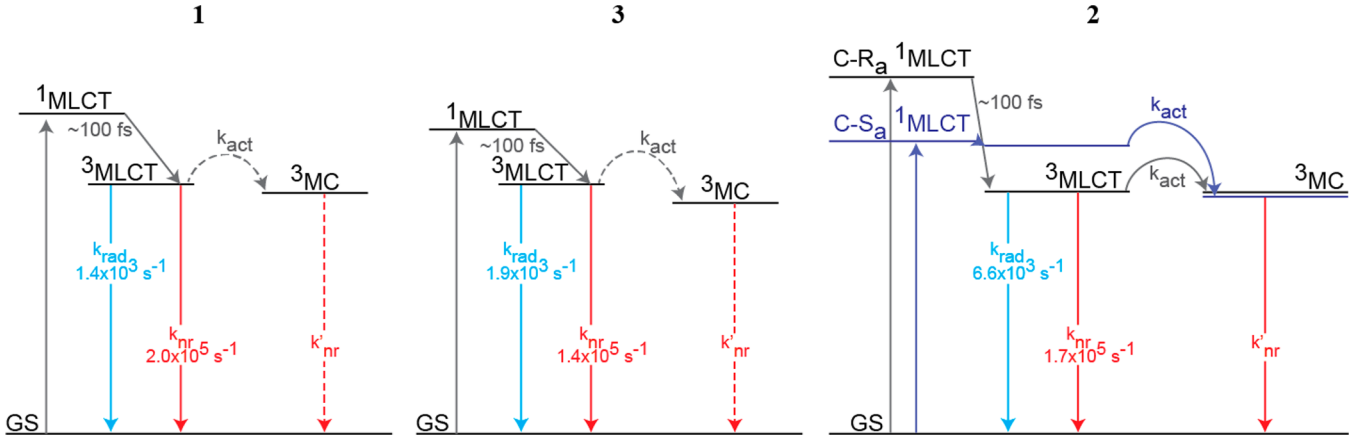

Figure 5. Jablonski diagrams for each complex, where the measured lifetimes, rate constants, and paths observed are solid lines.

complex,[21,42] which agrees well with previously reported tighter binding of stronger chelating ligands.[63] The tight binding of the DQPz ligands even allows for a nonbond breaking interconversion between two isomers at room temperature.[18] Thus, we were not surprised that **2** showed no photochemical response in the presence of Cl^- (Figure S21) as it also had no response to the addition of triflic acid (TfOH).[21]

In contrast, the lack of room-temperature emission in conjunction with the low-lying, highly distorted, and large number of calculated MC states suggests that the bidentate complexes should be highly susceptible to photosubstitution of the ligands.[32,67] The photochemical chlorination of **1** and **3** in 0.01 M Cl^- (NaCl or HCl) in water was monitored by UV−vis spectroscopy (Figure 6). Subsequent to visible light (>455 nm) irradiation in the presence of HCl, **1** displays similar spectral features to that seen upon photoinduced ligand exchange with acetonitrile.[21] Irradiation of **3** in neat acetonitrile led to solvent−ligand exchange,[21] and the addition of triflic acid (TfOH) just makes the process clean and irreversible through protonation of the dissociated ligands.[21] In contrast, in the presence of HCl, the MLCT absorption band of **3** decreased and a red-shifted absorption band appeared, indicating coordination of Cl^-, in agreement with many chlorinated complexes.[15] In the presence of NaCl, **3** behaves similarly to what was observed in 0.01 M HCl, and only slight changes in reaction rates were observed. Quantum yields (using the earliest part of the delay trace in Figure S20) were determined to be ∼0.2% for both compounds in HCl and ∼0.1% when using NaCl.

Interestingly, the time trace following λ_{max} in HCl and NaCl of **1** (Figure S22) suggests two different reactions taking place, while only a slight change in reaction rate was observed for **3**. This implies that two different mechanisms are governing the chlorination reactions. This discrepancy in mechanism prompted us to investigate the concentration dependence of the chlorination in water by varying the HCl concentration (Figure 7), using solutions with 0.1, 0.01, 0.001, and 0.0001 M HCl, while the Ru−complex concentrations were in the 10 μM range. For **3**, single wavelength kinetics of the MLCT absorption decay suggested only a minor concentration dependence (with an isosbestic point at ∼490 nm, Figure S23), with no dependence on the Cl^- source. In contrast, the kinetics of the **1** reaction exhibited an acid concentration dependence, manifest in reaction rates as well as spectral shape

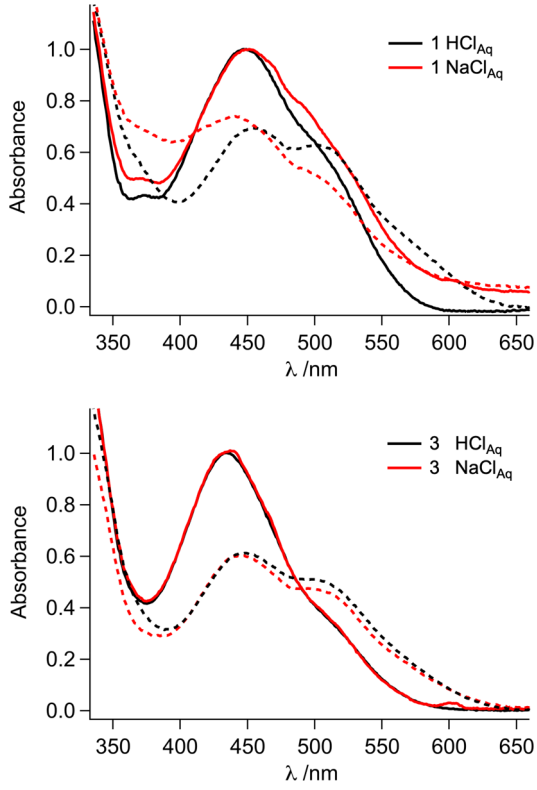

Figure 6. Absorption spectra of **1** (top) and **3** (bottom) before (solid) and after (dashed) visible light irradiation (>455 nm) in 0.01 M HCl_{Aq} (black) or 0.01 M $NaCl_{Aq}$ (red) in dionized (mQ) water with minimum 8MΩ/cm resistivity.

(with an isosbestic point at ∼520 nm, Figure S22). The absorption change of **1** is well modeled by a biexponential function, where the fast component increases and the slow component decreases with HCl concentration (Table S1). The slower component could probably correspond to solvent-coordination, which dominates the reaction between **1** and Cl^-, when TBACl or NaCl are used as Cl^- sources.[21]

These dynamics imply that the reaction rate and outcome of photochemical chlorination depend on competitive processes, such as partial photodissociation of a ligand, chlorination, solvent ligation, and protonation. The short lifetime of the MLCT state that seems to undergo this ligand exchange is perhaps indicative of an associative mechanism,[68] as the

DOI: 10.1021/acs.inorgchem.9b01543
Inorg. Chem. 2019, 58, 16354−16363

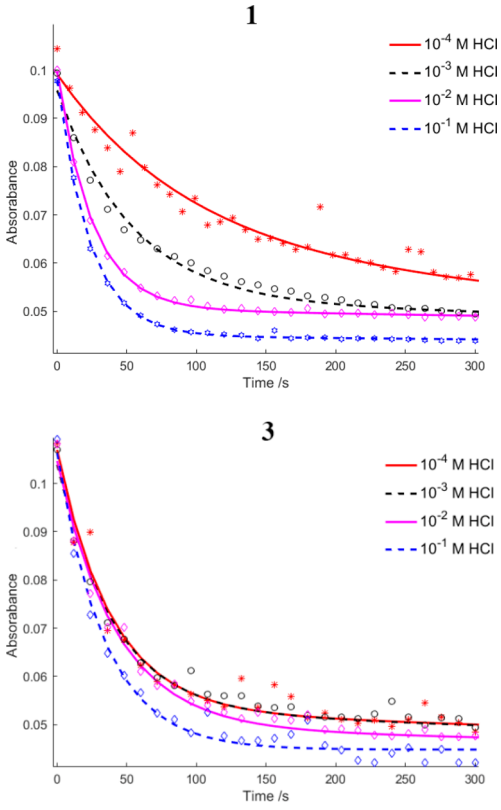

Figure 7. Comparison between photoinduced absorption change in H_2O/HCl for **1** (top) and **3** (bottom) when irradiated with visible light.

MLCT state is not dissociative in nature. Likely, a Ru−Cl bond would form before Ru−N dissociation via a preformed ion-pair. It is also possible that photoinitiated tautomerization reactions are involved, where a proton transfer can occur from the pyrazol to the photodissociated nitrogen. The fact that a lower pH increases the reaction rate of **1** in the presence of Cl^- and a higher pH results in excessive side reactions, likely with water, proves that the protonation dynamics are critical to its excited state reactivity.

CONCLUSIONS

This study provides detailed new insight into the multifaceted ultrafast dynamics of biheteroaromatic Ru complexes, which differ significantly from traditional Ru polypyridyl complexes. All three complexes, studied here, have ^{3}MLCT excited states as their lowest energy excited state with microsecond lifetimes (**2** > **3** > **1**) at 77 K. These ^{3}MLCT states are deactivated mostly through nonradiative pathways, with the tridentate complex decaying through a typical activated pathway via a ^{3}MC state and the bidentate complexes mostly deactivating directly to the GS. Contrary to the traditional picture of ligand exchange facilitated by the MC state, in these quinoline complexes, ligand exchange seems to occur in the complexes that decay directly to the GS from the MLCT and not in complex **2** which does populate an MC but is extremely photostable. In particular, **1** undergoes photoinduced ligand exchange with solvent or Cl^- in the presence of acid, and **3** undergoes a photoinduced ligand dissociation and coordination of multiple Cl^-, with no indication of the extremely extended bond distances required to stabilize a ^{3}MC state. In summary, the data presented here further emphasize the need for detailed understanding of structure−function relationships in transition metal complexes with new types of ligands.

ASSOCIATED CONTENT

Supporting Information

The Supporting Information is available free of charge at https://pubs.acs.org/doi/10.1021/acs.inorgchem.9b01543.

Temperature dependent absorption spectra, low temperature emission spectra, additional transient absorption spectra, Cl-reactivity absorption spectra, and photolysis parameters, as well as additional computational details including the spin densities and the potential energy slices of the triplet surfaces of each complex (PDF)

AUTHOR INFORMATION

Corresponding Author

*E-mail: abmaria@chalmers.se.

ORCID

Lisa A. Fredin: 0000-0002-4091-0899

Petter Persson: 0000-0001-7600-3230

Maria Abrahamsson: 0000-0002-6931-1128

Present Address

‖Department of Chemistry, Lehigh University, 6 E Packer Avenue, Bethlehem, PA 18015, USA

Author Contributions

⊥These authors contributed equally. The manuscript was written through contributions of all authors. All authors have given approval to the final version of the manuscript.

Notes

The authors declare no competing financial interest.

ACKNOWLEDGMENTS

We thank Ångpanneföreningens forskningsstiftelse (Åforsk), the Swedish Research Council (VR), the Crafoord Foundation, the Knut and Alice Wallenberg (KAW) Foundation, the Swedish Energy Agency (Energimyndigheten), as well as the Swedish Strategic Research Foundation (SSF) for financial support. M.A. and J.W. thank the Area of Advance Nano at Chalmers for financial support. P.P. acknowledges support from the NSC and LUNARC supercomputing facilities. L.A.F. acknowledges research computing resources provided by Lehigh University.

ABBREVIATIONS

Q3PzH, 8-(3-pyrazole)-quinoline; Q1Pz, 8-(1-pyrazole)-quinoline; DQPz, bis(quinolinyl)-1,3-pyrazole; MLCT, metal-to-ligand charge transfer; GS, ground state; MC, metal centered; Q, quinoline; Pz, pyrazolyl; tpy, 2,2′:6′,2″-terpyridine; py, pyridine; bpy, bipyridine; dmb, 4,4′-dimethyl-2,2′-bipyridine; biq, 2,2′-biquinoline; *mer*, meridional; OD, optical density; GTO, Gaussian type orbital; ECP, effective core potential; PCM, polarizable continuum model

REFERENCES

(1) Prier, C. K.; Rankic, D. A.; MacMillan, D. W. C. Visible Light Photoredox Catalysis with Transition Metal Complexes: Applications in Organic Synthesis. *Chem. Rev.* **2013**, *113*, 5322−5363.

(2) Tucker, J. W.; Stephenson, C. R. J. Shining Light on Photoredox Catalysis: Theory and Synthetic Applications. *J. Org. Chem.* **2012**, *77*, 1617−1622.

DOI: 10.1021/acs.inorgchem.9b01543
Inorg. Chem. 2019, 58, 16354−16363

(3) Younus, H. A.; Su, W.; Ahmad, N.; Chen, S.; Verpoort, F. Ruthenium Pincer Complexes: Synthesis and Catalytic Applications. *Adv. Synth. Catal.* **2015**, *357*, 283−330.
(4) Nazeeruddin, M. K.; Klein, C.; Liska, P.; Grätzel, M. Synthesis of Novel Ruthenium Sensitizers and Their Application in Dye-Sensitized Solar Cells. *Coord. Chem. Rev.* **2005**, *249*, 1460−1467.
(5) Bomben, P. G.; Robson, K. C. D.; Koivisto, B. D.; Berlinguette, C. P. Cyclometalated Ruthenium Chromophores for the Dye-Sensitized Solar Cell. *Coord. Chem. Rev.* **2012**, *256*, 1438−1450.
(6) Friedman, A. E.; Chambron, J. C.; Sauvage, J. P.; Turro, N. J.; Barton, J. K. A Molecular Light Switch for DNA: Ru(Bpy)2(Dppz)-2+. *J. Am. Chem. Soc.* **1990**, *112*, 4960−4962.
(7) Gill, M. R.; Thomas, J. A. Ruthenium (II) Polypyridyl Complexes and DNA—from Structural Probes to Cellular Imaging and Therapeutics. *Chem. Soc. Rev.* **2012**, *41*, 3179−3192.
(8) Yi, J. W.; Barry, N. P. E.; Furrer, M. A.; Zava, O.; Dyson, P. J.; Therrien, B.; Kim, B. H. Delivery of Floxuridine Derivatives to Cancer Cells by Water-Soluble Organometallic Cages. *Bioconjugate Chem.* **2012**, *23*, 461−471.
(9) Howerton, B. S.; Heidary, D. K.; Glazer, E. C. Strained Ruthenium Complexes Are Potent Light-Activated Anticancer Agents. *J. Am. Chem. Soc.* **2012**, *134*, 8324−8327.
(10) King, A. W.; Wang, L.; Rack, J. J. Excited State Dynamics and Isomerization in Ruthenium Sulfoxide Complexes. *Acc. Chem. Res.* **2015**, *48*, 1115−1122.
(11) Abrahamsson, M.; Jäger, M.; Österman, T.; Eriksson, L.; Persson, P.; Becker, H.-C.; Johansson, O.; Hammarström, L. A 3.0 Ms Room Temperature Excited State Lifetime of a Bistridentate RuII-Polypyridine Complex for Rod-Like Molecular Arrays. *J. Am. Chem. Soc.* **2006**, *128*, 12616−12617.
(12) Abrahamsson, M.; Becker, H. C.; Hammarström, L.; Bonnefous, C.; Chamchoumis, C.; Thummel, R. P. Six-Membered Ring Chelate Complexes of Ru(II): Structural and Photophysical Effects. *Inorg. Chem.* **2007**, *46*, 10354−10364.
(13) Abrahamsson, M.; Wolpher, H.; Johansson, O.; Larsson, J.; Kritikos, M.; Eriksson, L.; Norrby, P.-O. O.; Bergquist, J.; Sun, L.; Åkermark, B.; et al. A New Strategy for the Improvement of Photophysical Properties in Ruthenium(II) Polypyridyl Complexes. Synthesis and Photophysical and Electrochemical Characterization of Six Mononuclear Ruthenium(II) Bisterpyridine-Type Complexes. *Inorg. Chem.* **2005**, *44*, 3215−3225.
(14) Balzani, S. C. *Photochemistry and Photophysics of Coordination Compounds I*; Balzani, S. C., Ed.; Springer: Berlin, 2007; Vol. *280*.
(15) Juris, A.; Balzani, V.; Barigelletti, F.; Campagna, S.; Belser, P.; von Zelewsky, A. Ru(II) Polypyridine Complexes: Photophysics, Photochemistry, Eletrochemistry, and Chemiluminescence. *Coord. Chem. Rev.* **1988**, *84*, 85−277.
(16) McCusker, J. K. Femtosecond Absorption Spectroscopy of Transition Metal Charge-Transfer Complexes. *Acc. Chem. Res.* **2003**, *36*, 876−887.
(17) Hammarström, L.; Barigelletti, F.; Flamigni, L.; Indelli, M. T.; Armaroli, N.; Calogero, G.; Guardigli, M.; Sour, A.; Collin, J.-P.; Sauvage, J.-P. A Study on Delocalization of MLCT Excited States by Rigid Bridging Ligands in Homometallic Dinuclear Complexes of Ruthenium(II). *J. Phys. Chem. A* **1997**, *101*, 9061−9069.
(18) Caspar, J. V.; Meyer, T. J. Application of the Energy Gap Law to Nonradiative, Excited-State Decay. *J. Phys. Chem.* **1983**, *87*, 952−957.
(19) Caspar, J. V.; Kober, E. M.; Sullivan, B. P.; Meyer, T. J. Application of the Energy Gap Law to the Decay of Charge-Transfer Excited States. *J. Am. Chem. Soc.* **1982**, *104*, 630−632.
(20) Halcrow, M. A. Recent Advances in the Synthesis and Applications of 2,6-Dipyrazolylpyridine Derivatives and Their Complexes. *New J. Chem.* **2014**, *38*, 1868−1882.
(21) Hedberg Wallenstein, J.; Fredin, L. A.; Jarenmark, M.; Abrahamsson, M.; Persson, P. Chemical Consequences of Pyrazole Orientation in RuII Complexes of Unsymmetric Quinoline-Pyrazole Ligands. *Dalt. Trans.* **2016**, *45*, 11723−11732.
(22) Metherell, A. J.; Cullen, W.; Stephenson, A.; Hunter, C. A.; Ward, M. D. Fac and Mer Isomers of Ru(II) Tris(Pyrazolyl-Pyridine) Domplexes as Models for the Vertices of Coordination Cages: Structural Characterisation and Hydrogen-Bonding Characteristics. *Dalt. Trans.* **2014**, *43*, 71−84.
(23) Jarenmark, M.; Fredin, L. A.; Hedberg, J. H. J.; Doverbratt, I.; Persson, P.; Abrahamsson, M. A Homoleptic Trisbidentate Ru(II) Complex of a Novel Bidentate Biheteroaromatic Ligand Based on Quinoline and Pyrazole Groups: Structural, Electrochemical, Photophysical, and Computational Characterization. *Inorg. Chem.* **2014**, *53*, 12778−12790.
(24) Jarenmark, M.; Carlström, G.; Fredin, L. A.; Hedberg Wallenstein, J.; Doverbratt, I.; Abrahamsson, M.; Persson, P. Diastereomerization Dynamics of a Bistridentate RuII Complex. *Inorg. Chem.* **2016**, *55*, 3015−3022.
(25) Tseng, H.-W.; Zong, R.; Muckerman, J. T.; Thummel, R. Mononuclear Ruthenium(II) Complexes That Catalyze Water Oxidation. *Inorg. Chem.* **2008**, *47*, 11763−11773.
(26) Zong, R.; Thummel, R. P. A New Family of Ru Complexes for Water Oxidation. *J. Am. Chem. Soc.* **2005**, *127*, 12802−12803.
(27) Gil-Sepulcre, M.; Böhler, M.; Schilling, M.; Bozoglian, F.; Bachmann, C.; Scherrer, D.; Fox, T.; Spingler, B.; Gimbert-Suriñach, C.; Alberto, R.; et al. Ruthenium Water Oxidation Catalysts Based on Pentapyridyl Ligands. *ChemSusChem* **2017**, *10*, 4517−4525.
(28) Garner, R. N.; Joyce, L. E.; Turro, C. Effect of Electronic Structure on the Photoinduced Ligand Exchange of Ru(II) Polypyridine Complexes. *Inorg. Chem.* **2011**, *50*, 4384−4391.
(29) Raber, M. M.; Brady, M. D.; Troian-Gautier, L.; Dickenson, J. C.; Marquard, S. L.; Hyde, J. T.; Lopez, S. J.; Meyer, G. J.; Meyer, T. J.; Harrison, D. P. Fundamental Factors Impacting the Stability of Phosphonate-Derivatized Ruthenium Polypyridyl Sensitizers Adsorbed on Metal Oxide Surfaces. *ACS Appl. Mater. Interfaces* **2018**, *10*, 22821−22833.
(30) Knoll, J. D.; Albani, B. A.; Durr, C. B.; Turro, C. Unusually Efficient Pyridine Photodissociation from Ru (II) Complexes with Sterically Bulky Bidentate Ancillary Ligands. *J. Phys. Chem. A* **2014**, *118*, 10603−10610.
(31) Ravi Kishore, V. V. N.; Narasimhan, K. L.; Periasamy, N. On the Radiative Lifetime, Quantum Yield and Fluorescence Decay of Alq in Thin Films. *Phys. Chem. Chem. Phys.* **2003**, *5*, 1386−1391.
(32) Caspar, J. V.; Meyer, T. J. Photochemistry of MLCT Excited States. Effect of Nonchromophoric Ligand Variations on Photophysical Properties in the Series Cis-Ru(Bpy)2L22+. *Inorg. Chem.* **1983**, *22*, 2444−2453.
(33) Kober, E. M.; Caspar, J. V.; Lumpkin, R. S.; Meyer, T. J. Application of the Energy Gap Law to Excited-State Decay of Osmium(II)-Polypyridine Complexes: Calculation of Relative Nonradiative Decay Rates from Emission Spectral Profiles. *J. Phys. Chem.* **1986**, *90*, 3722−3734.
(34) Lumpkin, R. S.; Meyer, T. J. Effect of the Glass-to-Fluid Transition on Excited-State Decay. Application of the Energy Gap Law. *J. Phys. Chem.* **1986**, *90*, 5307−5312.
(35) Treadway, J. A.; Loeb, B.; Lopez, R.; Anderson, P. A.; Keene, F. R.; Meyer, T. J. Effect of Delocalization and Rigidity in the Acceptor Ligand on MLCT Excited-State Decay. *Inorg. Chem.* **1996**, *35*, 2242−2246.
(36) Timpson, C. J.; Bignozzi, C. A.; Sullivan, B. P.; Kober, E. M.; Meyer, T. J. Influence of Solvent on the Spectroscopic Properties of Cyano Complexes of Ruthenium(II). *J. Phys. Chem.* **1996**, *100*, 2915−2925.
(37) Perdew, J. P.; Burke, K.; Ernzerhof, M. Generalized Gradient Approximation Made Simple. *Phys. Rev. Lett.* **1996**, *77*, 3865; *Phys. Rev. Lett.* **1997**, *78*, 1396.
(38) Perdew, J. P.; Burke, K.; Ernzerhof, M. Generalized Gradient Approximation Made Simple. *Phys. Rev. Lett.* **1996**, *77*, 3865−3868.
(39) Adamo, C.; Barone, V. Toward Reliable Density Functional Methods Without Adjustable Parameters: The PBE0Model. *J. Chem. Phys.* **1999**, *110*, 6158−6170.

DOI: 10.1021/acs.inorgchem.9b01543
Inorg. Chem. 2019, 58, 16354−16363

(40) Dolg, M.; Wedig, U.; Stoll, H.; Preuss, H. Energy-adjusted Abinitio Pseudopotentials for the First Row Transition Elements. *J. Chem. Phys.* **1987**, *86*, 866.
(41) *Gaussian 09*, Revision D.01; Gaussian Inc.: Wallingford, CT, 2016.
(42) Abrahamsson, M.; Jäger, M.; Kumar, R. J.; Österman, T.; Persson, P.; Becker, H.-C. C.; Johansson, O.; Hammarström, L. Bistridentate Ruthenium(II)Polypyridyl-Type Complexes with Microsecond 3MLCT State Lifetimes: Sensitizers for Rod-Like Molecular Arrays. *J. Am. Chem. Soc.* **2008**, *130*, 15533−15542.
(43) Abrahamsson, M.; Becker, H.-C.; Hammarström, L. Microsecond 3MLCT Excited State Lifetimes in Bis-Tridentate Ru(II)-Complexes: Significant Reductions of Non-Radiative Rate Constants. *Dalt. Trans.* **2017**, *46*, 13314−13321.
(44) Wallin, S.; Davidsson, J.; Modin, J.; Hammarström, L. Femtosecond Transient Absorption Anisotropy Study on [Ru(Bpy)-3]2+ and [Ru(Bpy)(Py)4]2+. Ultrafast Interligand Randomization of the MLCT State. *J. Phys. Chem. A* **2005**, *109*, 4697−4704.
(45) Damrauer, N. H.; Cerullo, G.; Yeh, A.; Boussie, T. R.; Shank, C. V.; McCusker, J. K. Femtosecond Dynamics of Excited-State Evolution in $[Ru(Bpy)_3]^{2+}$. *Science (Washington, DC, U. S.)* **1997**, *275*, 54−57.
(46) Sun, H.; Hoffman, M. Z. Photophysics of Ruthenium(II)-Diimine Complexes in Water-Acetonitrile Mixed Solvents. *J. Phys. Chem.* **1993**, *97*, 11956−11959.
(47) Kreitner, C.; Heinze, K. Excited State Decay of Cyclometalated Polypyridine Ruthenium Complexes: Insight from Theory and Experiment. *Dalt. Trans.* **2016**, *45*, 13631−13647.
(48) Soupart, A.; Alary, F.; Heully, J. L.; Elliott, P. I. P.; Dixon, I. M. Exploration of Uncharted 3PES Territory for [Ru(Bpy)3]2+: A New 3MC Minimum Prone to Ligand Loss Photochemistry. *Inorg. Chem.* **2018**, *57*, 3192−3196.
(49) Soupart, A.; Dixon, I. M.; Alary, F.; Heully, J. L. DFT Rationalization of the Room-Temperature Luminescence Properties of Ru(Bpy) 32+ and Ru(Tpy) 22+: 3MLCT-3MC Minimum Energy Path from NEB Calculations and Emission Spectra from VRES Calculations. *Theor. Chem. Acc.* **2018**, *137*, 1−11.
(50) Fredin, L. A. L. a.; Pápai, M.; Rozsályi, E.; Vankó, G.; Wärnmark, K.; Sundström, V.; Persson, P. Exceptional Excited-State Lifetime of an Iron(II)- N -Heterocyclic Carbene Complex Explained. *J. Phys. Chem. Lett.* **2014**, *5*, 2066−2071.
(51) Osterman, T.; Abrahamsson, M.; Becker, H.-C.; Hammarstrom, L.; Persson, P. Influence of Triplet State Multidimensionality on Excited State Lifetimes of Bis-Tridentate RuII Complexes: A Computational Study. *J. Phys. Chem. A* **2012**, *116*, 1041−1050.
(52) Parada, G. A.; Fredin, L. A.; Santoni, M. P.; Jäger, M.; Lomoth, R.; Hammarström, L.; Johansson, O.; Persson, P.; Ott, S. Tuning the Electronics of Bis(Tridentate)Ruthenium(II) Complexes with Long-Lived Excited States: Modifications to the Ligand Skeleton beyond Classical Electron Donor or Electron Withdrawing Group Decorations. *Inorg. Chem.* **2013**, *52*, 5128−5137.
(53) Wagenknecht, P. S.; Ford, P. C. Metal Centered Ligand Field Excited States: Their Roles in the Design and Performance of Transition Metal Based Photochemical Molecular Devices. *Coord. Chem. Rev.* **2011**, *255*, 591−616.
(54) Englman, R.; Jortner, J. The Energy Gap Law for Radiationless Transitions in Large Molecules. *Mol. Phys.* **1970**, *18*, 145−164.
(55) Crosby, G. A. Spectroscopic Investigations of Excited States of Transition-Metal Complexes. *Acc. Chem. Res.* **1975**, *8*, 231−238.
(56) Crosby, G. A.; Watts, R. J.; Carstens, D. H. W. Inversion of Excited States of Transition-Metal Complexes. *Science* **1970**, *170*, 1195−1196.
(57) Sprouse, S.; King, K. A.; Spellane, P. J.; Watts, R. J. Photophysical Effects of Metal-Carbon σ Bonds in Ortho-Metalated Complexes of Ir(III) and Rh(III). *J. Am. Chem. Soc.* **1984**, *106*, 6647−6653.
(58) King, K. A.; Spellane, P. J.; Watts, R. J. Excited-State Properties of a Triply Ortho-Metalated Iridium(III) Complex. *J. Am. Chem. Soc.* **1985**, *107*, 1431−1432.
(59) DeArmond, M. K. Relaxation of Excited States in Transition-Metal Complexes. *Acc. Chem. Res.* **1974**, *7*, 309−315.
(60) Caspar, J. V.; Westmoreland, T. D.; Allen, G. H.; Meyer, T. J.; Bradley, P. G.; Woodruff, W. H. Molecular and Electronic Structure in the Metal-to-Ligand Charge-Transfer Excited States of D6Transition-Metal Complexes in Solution. *J. Am. Chem. Soc.* **1984**, *106*, 3492−3500.
(61) Ohsawa, Y.; Sprouse, S.; King, K. A.; DeArmond, M. K.; Hanck, K. W.; Watts, R. J. Electrochemistry and Spectroscopy of Ortho-Metalated Complexes of Ir(III) and Rh(III). *J. Phys. Chem.* **1987**, *91*, 1047−1054.
(62) Maestri, M.; Sandrini, D.; Balzani, V.; Chassot, L.; Jolliet, P.; Von Zelewsky, A. Luminescence of Ortho-Metallated Platinum(II) Complexes. *Chem. Phys. Lett.* **1985**, *122*, 375−379.
(63) Breivogel, A.; Wooh, S.; Dietrich, J.; Kim, T. Y.; Kang, Y. S.; Char, K.; Heinze, K. Anchor-Functionalized Push-Pull-Substituted Bis(Tridentate) Ruthenium(II) Polypyridine Chromophores: Photostability and Evaluation as Photosensitizers. *Eur. J. Inorg. Chem.* **2014**, *2014*, 2720−2734.
(64) Fredin, L. A.; Persson, P. Influence of Triplet Surface Properties on Excited-State Deactivation of Expanded Cage Bis(Tridentate)-Ruthenium(II) Complexes. *J. Phys. Chem. A* **2019**, *123*, 5293−5299.
(65) Otto, S.; Förster, C.; Wang, C.; Resch-Genger, U.; Heinze, K. A Strongly Luminescent Chromium(III) Complex Acid. *Chem. - Eur. J.* **2018**, *24*, 12555−12563.
(66) Breivogel, A.; Meister, M.; Förster, C.; Laquai, F.; Heinze, K. Excited State Tuning of Bis(Tridentate) Ruthenium(II) Polypyridine Chromophores by Push-Pull Effects and Bite Angle Optimization: A Comprehensive Experimental and Theoretical Study. *Chem. - Eur. J.* **2013**, *19*, 13745−13760.
(67) Rillema, D. P.; Taghdiri, D. G.; Jones, D. S.; Worl, L. A.; Meyer, T. J.; Levy, H. A.; Keller, C. D. Structure and Redox and Photophysical Properties of a Series of Ruthenium Heterocycles Based on the Ligand 2,3-Bis(2-Pyridyl)Quinoxaline. *Inorg. Chem.* **1987**, *26*, 578−585.
(68) Crabtree, R. H. Carbonyls, Phosphine Complexes, and Ligand Substitution Reactions. In *Organometallic Chemistry of the Transition Metals*; John Wiley & Sons, Inc., 2005; pp 87−124.

DOI: 10.1021/acs.inorgchem.9b01543
Inorg. Chem. 2019, 58, 16354−16363